

Synthesis, spectroscopic characterisation and biological activity studies of Co(II), Ni(II), Cu(II) and Zn(II) metal complexes with azo dye ligand derived from 4,4'-diaminodiphenylether and 5-sulpho salicylic acid

S. N. Chaulia

P. G. Department of Chemistry, G. M. (AUTO) College, Sambalpur, Odisha (INDIA)

Received February 16, 2016; Revised May 27, 2016

A series of metal complexes of Co(II), Ni(II), Cu(II) and Zn(II) have been synthesized with a new azo dye ligand 4,4'-bis(2'-hydroxy-3'-carboxy-5'-sulphophenylazo)diphenylether derived from 4,4'-diaminodiphenyl ether and 5-sulpho salicylic acid. The metal complexes along with the ligand have been characterised by analytical, molar conductance, magnetic susceptibility measurement, IR, NMR, electronic, ESR, mass spectra and thermal study. The analytical and spectral data predicts octahedral for Co(II), Ni(II), distorted octahedral geometry for Cu(II) complexes and tetrahedral geometry for Zn(II) complex. Computational study of the ligand and the metal complexes has been made to determine the geometrical parameters and the global reactive descriptors. The XRD (powder pattern) indicates orthorhombic crystal system for the Cu(II) complex. The thermal study reveals thermal stability of the complexes and the fluorescence study predicts photoactive properties of the azo compounds. The SEM image of the Zn(II) complex provides its information about its surface morphology. The Biological study indicates the antibacterial properties and DNA binding activity of the newly synthesised compounds.

Keywords: Computational study, Biological study, Azo compounds, SEM image

INTRODUCTION

Azo compounds constitute the largest class of synthesised organic dyes and azo dyes and their metal complexes have been attracting the attention of researchers due to their versatile application in various fields. In addition to the traditional uses of dyes as dyeing agents[1], laboratory reagents[2], these compounds are also used in biomedical studies as antibacterial, antifungal, antitumor agents etc [3,4] and high technology areas including textiles, paper, leather and electro-optical devices[5,6]. The Azo compounds derived from 4,4'-diaminodiphenyl ether and its complexes have evoked great interest in recent years due to its antibacterial properties and its application in the making of thermally stable materials that can be used in the field of adsorption and catalysis[7,8], that encouraged me to prepare azo dye from 4,4'-diaminodiphenylether and 5-sulpho salicylic acid, its metal complexes, to characterise the compounds by various physico-chemical and spectral techniques and to evaluate their biological activities.

EXPERIMENTAL

Materials and Measurements

All chemical and solvents used in this investigation are analytical grade provided by

Himedia and double distilled deionised water was used during the experiments. Elemental analysis of the ligand and complexes was carried out by Perkin-Elmer elemental analyser, cobalt, nickel, copper and Zn contents were determined by Perkin-Elmer 2380 atomic absorption spectrometer and chloride content was estimated by standard procedure, Systronic conductivity bridge 30 was used to measure molar conductance of the complexes, Magnetic susceptibility of the complexes was measured by Guoy's balance using $\text{Hg}[\text{Co}(\text{NCS})_4]$ as a calibrant at room temperature, IR spectra of the ligand and metal complexes were recorded using KBr pellets by Perkin-Elmer FT-IR spectrometer within the range 4000- 450 cm^{-1} , UV-Visible spectra of the complexes were collected using a THERMO SPECTRONIC 6 HEXIOS α and fluorescence spectra were recorded in a Fluorescence spectrometer, ^1H NMR spectra of the ligand and the Zn(II) complex were obtained from 500 MHz- NMR spectrometer using TMS as reference, ESR spectrum of the Cu(II) complex was recorded on spectrum of the Cu(II) complex was recorded on JES-FA 200 ESR spectrometer, Mass spectra of the ligand and its complexes were recorded through JEOL GC-MS Mass Spectrometer, thermal study of the metal complex was done by NETZSCH STA 449 F3 JUPITOR, SEM image of the complexes were taken in JES FA 200, the XRD powder pattern of the Cu(II) complex was collected using a Philips X'Pert Pro diffractometer.

* To whom all correspondence should be sent:
E-mail: satyanarayanchaulia@gmail.com

In order to get the better picture about reactivity and geometrical parameters, computational study of the ligand and the metal complexes was performed by Gaussian 03 software package[9].

The DNA binding study of the azo compounds was made by Gel electrophoresis method [10]. 10 μL of the metal complexes was taken along with 15 μL of CT DNA solution dissolved in Tris-EDTA in centrifuge tubes. The tubes were incubated at 37°C for 1 hour. After incubation, the tubes containing solution were kept in a refrigerator at 0°C for few minutes, 5 μL gel loading buffer with tracking dye (0.25% bromo phenol) was taken in the tubes for electrophoresis. The electrophoresis was continued under constant voltage (50 V) and photographed under UV illumination.

Hydrodynamic volume change [11] was observed by Ostwald Viscometer immersed in a thermostatic bath maintained at 37°C. A digital stopwatch was used to measure the flow time, mixing of complexes under investigation with CT-DNA was carried out by bubbling nitrogen. Data were presented by plotting a graph indicating $(\eta/\eta_0)^{1/3}$ versus [complex]/[DNA] where η is the viscosity of DNA in presence of complexes and η_0 represents the viscosity of DNA alone.

The antibacterial activity of the ligand and its metal complexes was studied in vitro by the cup-plate method [12] against the *Escherichia coli* (MTCC 40) and *Staphylococcus aureus* (MTCC 87) using agar nutrient as the medium. The investigated ligand and its complexes were

dissolved in DMF. The sterilised agar plates were swabbed with the bacteria culture and filled with test solutions, then incubated at 37 °C for 24 h. The activity was evaluated by measuring the zone of inhibition with respect to the standard drug Tetracycline.

Synthesis of the ligand

The ligand is synthesised by the coupling reaction between diazonium chloride solution derived from 4,4'-diaminodiphenylether and the alkaline solution of 5-sulphosalicylic acid. The diazonium chloride solution was prepared by the dissolution of 4,4'-diaminodiphenylether(0.01 mol, 2.0 gram) in hydrochloric acid and adding equivalent sodium nitrite solution at 0 – 5 °C with vigorous stirring, The ice-cooled diazonium chloride solution was added to added to alkaline solution of 5-sulphosalicylic acid(0.02 mol, 4.02 gram). The coloured azo compound produced again recrystallised from ethanol (Fig. 1.).

Preparation of metal complexes

The metal chlorides in ethanol solution were mixed with DMF solution of the ligand separately and the reaction mixture was refluxed for one hour at 60 °C. The solution is allowed to cool and concentrated Ammonia solution was added drop wise to the solution with stirring till the formation of complex compounds. The solid (Fig. 3, 4) complexes thus separated were washed with alcohol and dried in vacuum (Fig. 2).

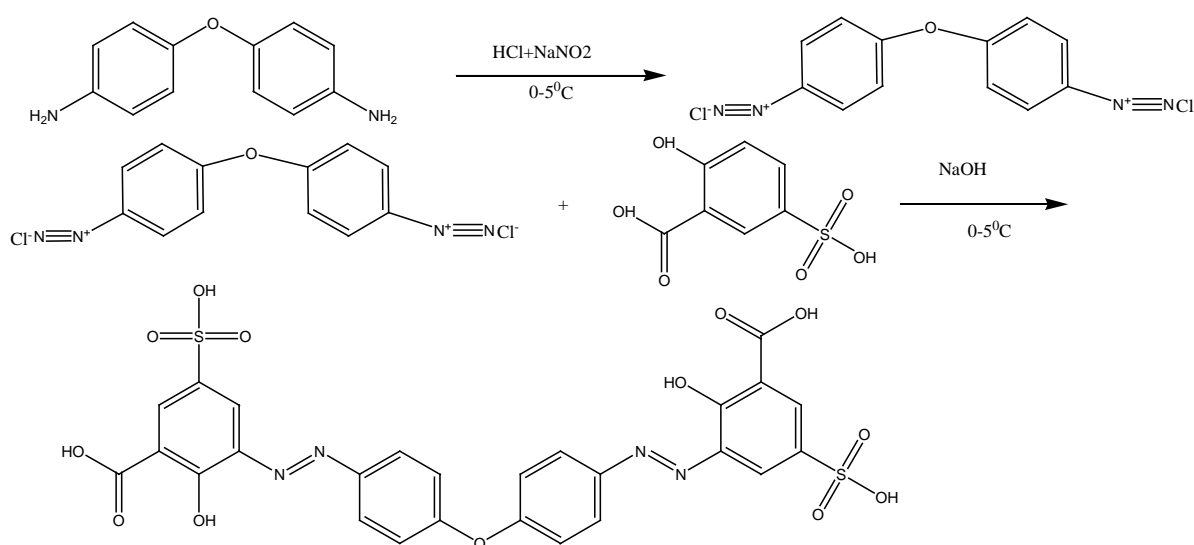


Fig. 1. Reaction scheme-1.



M= Co(II), Ni(II) and Cu(II)



M'= Zn(II)

Fig. 2. Reaction scheme-2.

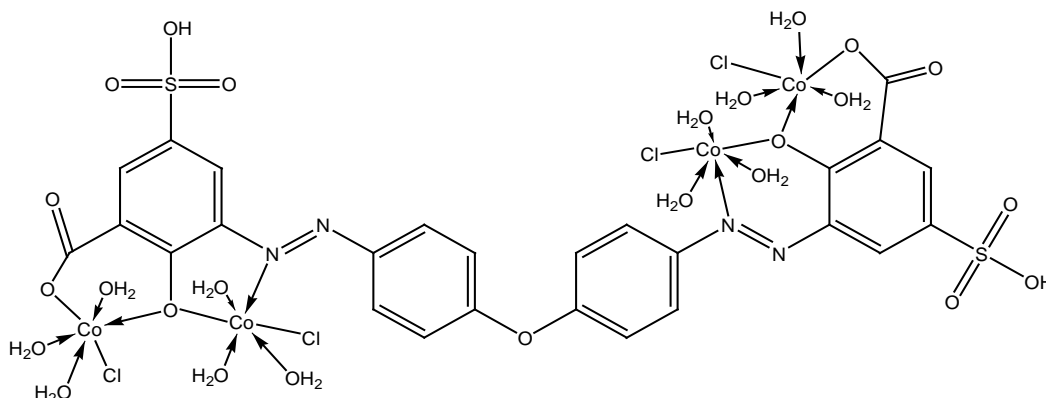


Fig. 3. Structure of Co(II) complex.

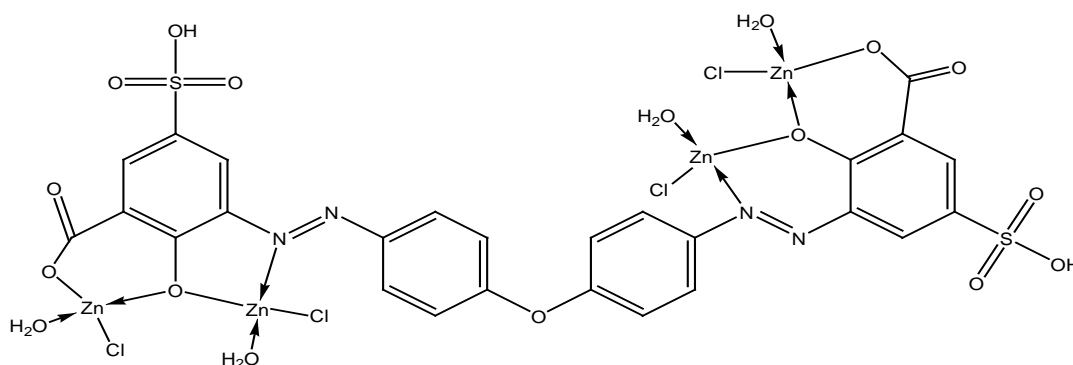


Fig. 4. Structure of Zn(II) complex.

RESULTS AND DISCUSSION

The analytical and physical properties of the Azo dye and its complexes are in good agreement with calculated values (Table 1). The analytical data of the complexes are consistent with the general formula $[M_4LCl_4(H_2O)_{12}]$ for Co(II), Ni(II), Cu(II) and $[M'_4LCl_4(H_2O)_4]$. The molar conductance of the complexes with 1×10^{-3} M DMSO solution are found to be in the range of 9.1-12.5 $\text{ohm}^{-1}\text{cm}^2\text{mol}^{-1}$ indicating non-electrolytic nature[13]. All compounds are insoluble in ethanol, methanol, acetone, ether, and chloroform but soluble in DMF and DMSO.

IR study

The IR spectrum of the ligand (Fig. 5) is compared with the spectra of metal complexes (Fig. 6) in order to examine the mode of bonding between ligand and complexes (Table 2). The IR spectrum of the ligand shows a broad band at 3422 cm^{-1} which is missing from the spectra of the metal complexes that indicates deprotonation of phenolic(-OH) and bonding of metal atoms with oxygen atom of the -OH group. The C-O frequency vibration band observed at 1268 cm^{-1} in ligand is shifted to $\sim 1235 \text{ cm}^{-1}$ in complexes confirming bonding of metal atoms with oxygen atom of -OH group[14]. Two bands appear at 1383 and 1589 cm^{-1} corresponds to ν_{sym} and ν_{asym} respectively in the spectrum of the ligand which are observed at 1279 cm^{-1} and 1581 cm^{-1} due to ν_{sym} and ν_{asym} that

indicates monodentate nature of the carboxylate group and bonding of carboxylic oxygen with metal atoms[15]. A band appears at 1491 cm^{-1} corresponds to -N=N- group in the ligand is shifted to $\sim 1489 \text{ cm}^{-1}$ in metal complexes that suggests bonding of azo nitrogen with the metal ions[16].The peak at 1657 cm^{-1} in ligand confirms the presence carbonyl group of ethanoyl group of the ligand which is shifted to 1649 cm^{-1} in metal complexes that indicates bonding of carbonyl oxygen atom with the metal ions. The spectra of

complexes reveal the presence of band at $\sim 3512 \text{ cm}^{-1}$ due to the vibrational frequency of O-H of coordinated/ lattice held water. The presence of coordinated water is further confirmed by the rocking band at $\sim 836 \text{ cm}^{-1}$ and twisting band at $\sim 780 \text{ cm}^{-1}$ [17].The vibrational frequencies of M-O and M-N bonds which appear at $\sim 589 \text{ cm}^{-1}$ and $\sim 489 \text{ cm}^{-1}$ respectively confirm the bonding between metal ions with the ligand through phenolic oxygen and azo nitrogen atoms[18].

Table 1. Analytical data of the ligand and its metal complexes

comp	Colour	M.P. (°C)	% Found(calcd)					
			M	C	H	N	Cl	S
LH ₄	Brick Red	85	-	47.15	2.32	8.29	-	9.43
				(47.42)	(2.75)	(8.51)		(9.7)
[Co ₄ LCl ₄ (H ₂ O) ₁₂]	Reddish brown	>300	18.43	24.87	3.01	4.12	11.03	4.96
			(18.88)	(25.02)	(3.07)	(4.49)	(11.37)	(5.14)
[Ni ₄ LCl ₄ (H ₂ O) ₁₂]	Red	>300	18.39	24.76	2.99	4.33	11.11	4.94
			(18.82)	(25.04)	(3.07)	(4.49)	(11.37)	(5.14)
[Cu ₄ LCl ₄ (H ₂ O) ₁₂]	Brown	>300	19.89	24,53	2.86	4.21	11.07	4.65
			(20.07)	(24.65)	(3.02)	(4.42)	(11.20)	(5.06)
[Zn ₄ LCl ₄ (H ₂ O) ₄]	Light red	>300	22.87	27.33	1,75	4.75	12,14	5.43
			(23.15)	(27.64)	(1.96)	(4.96)	(12.55)	(5.68)

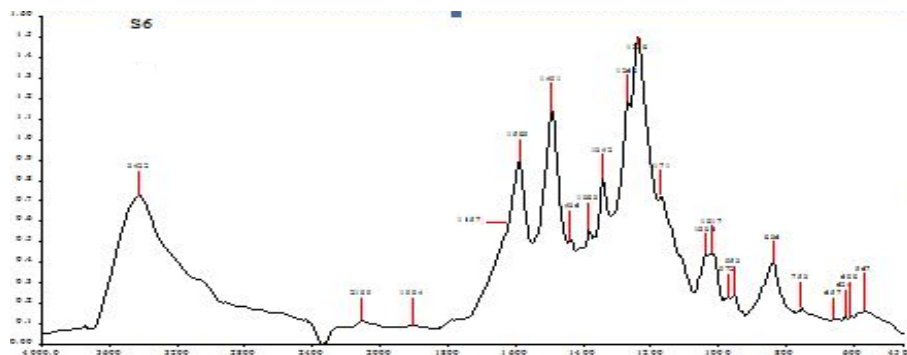


Fig. 5. IR Spectrum of the ligand.

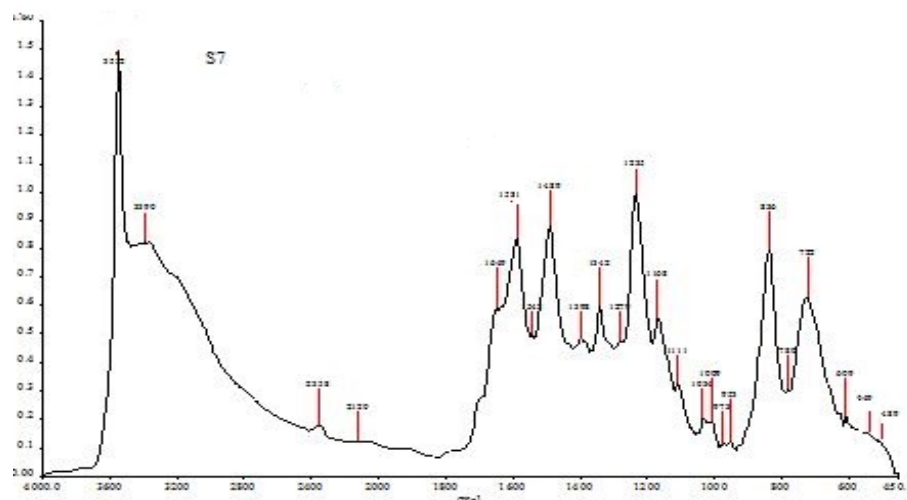


Fig. 6. IR Spectrum of the Co(II) complex

Table 2. IR data of the investigating compounds

compound	$\nu(\text{C-O})$ cm^{-1}	$\nu(\text{N=N})$ cm^{-1}	$\nu(\text{COO}^-)_{\text{sym}}$ cm^{-1}	$\nu(\text{COO}^-)_{\text{asym}}$ cm^{-1}	$\nu(\text{M-O})$ cm^{-1}	$\nu(\text{M-N})$ cm^{-1}
1	1268	1491	1383	1589	-	-
2	1235	1489	1279	1581	589	489
3	1234	1488	1278	1580	588	489
4	1235	1488	1279	1581	588	489
5	1236	1489	1278	1580	589	488

1-LH₄, 2- Co(II) complex, 3-Ni(II)complex, 3- Cu(II) complex and 4- Zn(II) complex

Electronic spectra and magnetic measurement

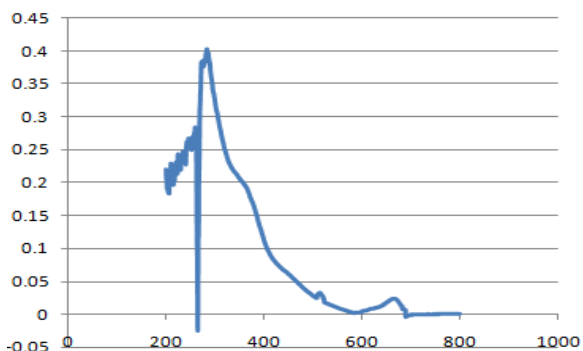
As synthesis of single crystals of the complexes has been failed, the electronic spectral and magnetic moment measurement data are used to confirm the geometry of the complexes (Table 3). Three d-d transition bands are observed in the Spectrum of Co(II) complex (Fig. 7.) at 13880, 16150, 26315 cm^{-1} corresponding to ${}^4\text{T}_{1g}(\text{F}) \rightarrow {}^4\text{T}_{2g}(\text{F}), {}^4\text{T}_{1g}(\text{F}) \rightarrow {}^4\text{A}_{2g}(\text{F}), {}^4\text{T}_{1g}(\text{F}) \rightarrow {}^4\text{T}_{2g}(\text{P})$ that indicates octahedral geometry of the complex [19]. The electronic parameters of the Co(II) complex were calculated by using the following equations.

$$Dq = \nu_2 - \nu_1/10$$

$$B = \nu_2 + \nu_3 - 3 \nu_1/15$$

$$\beta_{35} = B/971$$

$$\% \text{ of } \beta_{35} = (\beta^0) = (1 - \beta_{35})100$$

**Fig. 7.** Electronic Spectrum of the Co(II) complex.

In the Ni(II) complex (Fig. 8) also three bands are observed at 14705, 18867, 25641 cm^{-1} due to ${}^3\text{A}_{2g}(\text{F}) \rightarrow {}^3\text{T}_{2g}(\text{F}), {}^3\text{A}_{2g}(\text{F}) \rightarrow {}^3\text{T}_{1g}(\text{F}), {}^3\text{A}_{2g}(\text{F}) \rightarrow {}^3\text{T}_{1g}(\text{P})$ which arises from octahedral geometry [20]. The parameters of the complex were calculated by using the equations

$$Dq = \nu_2 - \nu_1/10$$

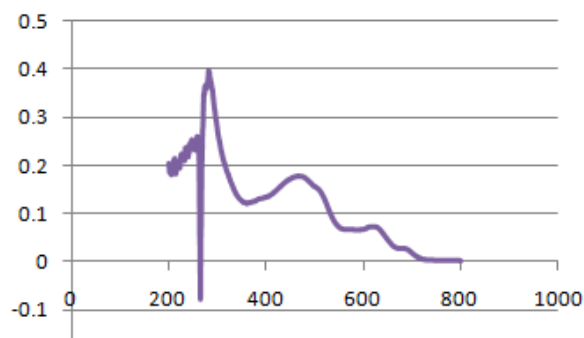
$$B = \nu_2 + \nu_3 - 3 \nu_1/15$$

$$\beta_{35} = B/1041$$

$$\% \text{ of } \beta_{35} = (\beta^0) = (1 - \beta_{35})100$$

The Racah parameter (B), Nephelauxetic effect (β), β^0 of Co(II) and Ni(II) complexes strongly indicate covalent bonding between ligand and metal ions. The value of ν_2/ν_1 for Co(II) and Ni(II) complexes was found to be 1.16 and 1.28

respectively which are close to the value expected from an octahedral geometry.

**Fig. 8.** Electronic Spectrum of the Ni(II) complex

The Cu(II) complex shows a d-d transition band at 15350 cm^{-1} which may be assigned to ${}^2\text{E}_g \rightarrow {}^2\text{T}_{2g}$ transition which favours a distorted octahedral geometry for the complex [22]. The magnetic susceptibility measurements of the metal complexes are undertaken to get information's regarding their structures. The magnetic moment of the Co(II), Ni(II) and Cu(II) complexes were found to be 1.38 B.M., 1.31 B.M. and 1.04 B.M. respectively in place of 3.87 B.M., 2.83 B.M. and 1.73 B.M. magnetic moment expected from an octahedral geometry. This sub-normality in magnetic moment of the investigating complexes may be due to interaction of electron spins of the neighbouring metal ions. This anti ferromagnetism due to pairing of electron spins may be due to super exchange through (M-O-M) [23,24]. The Zn(II) complex is found to be diamagnetic, hence tetrahedral geometry may be suggested based on the spectral and analytical data.

¹H NMR Study

The spectra of the ligand (Fig. 9) and Zn(II) complex (Fig. 10) are recorded in DMSO-d₆ solvent. The ¹H NMR spectrum of the ligand shows multiplet at δ 6.99-8.45 ppm which may be assigned to aromatic protons. The peaks at δ 10.21 ppm corresponds to phenolic (-OH) group and -CH₃ group is also confirmed by the presence of peak at δ 2.89 ppm [25].

The spectrum of Zn(II) complex is compared with the azo dye ligand and it is observed that the peak due to -OH group found in the ligand was absent in the complex. This indicates deprotonation of -OH group and formation of metal-O bond [26] in accordance with the data revealed by IR.

Mass spectra Study

As mass spectra of the compounds provides vital information for their structural elucidations,

the mass spectra of the ligand and its Co(II) (Fig. 11, 12) complexes are recorded to confirm their molecular mass and stoichiometric composition. The spectrum of the ligand shows the molecular ion peak at m/z 658.76 corresponding to the molecular mass of [C₂₆H₁₈N₄O₁₃S₂]. The spectrum of the Co(II) complex of the ligand gives molecular ion peak at m/z 1248.27 which confirms its proposed molecular formula as [M₄LCI₄(H₂O)₁₂]

Table 3. Electronic data of the metal complexes.

Compound	λ_{max} (cm ⁻¹)	Transitions	B	β_{35}	% of β_{35}	ν_2/ν_1	Geometry	μ_{eff} B.M.
1	13880	$^4T_{1g}(F) \rightarrow ^4T_{2g}(F)$	55	0.056		1.16	octahedral	1.38
	16150	$^4T_{1g}(F) \rightarrow ^4A_{2g}(F)$						
	26315	$^4T_{1g}(F) \rightarrow ^4T_{2g}(P)$						
	34482	CT						
2	14705	$^3A_{2g}(F) \rightarrow ^3T_{2g}(F)$	19.8	0.019		1.28	octahedral	1.31
	18867	$^3A_{2g}(F) \rightarrow ^3T_{1g}(F)$						
	25641	$^3A_{2g}(F) \rightarrow ^3T_{1g}(P)$						
	38461	CT						
3	15350	$^2E_g \rightarrow ^2T_{2g}$	-	-	-	-	Distorted octahedral	1.04

1-Co(II) complex, 2-Ni(II)complex, 3- Cu(II) complex

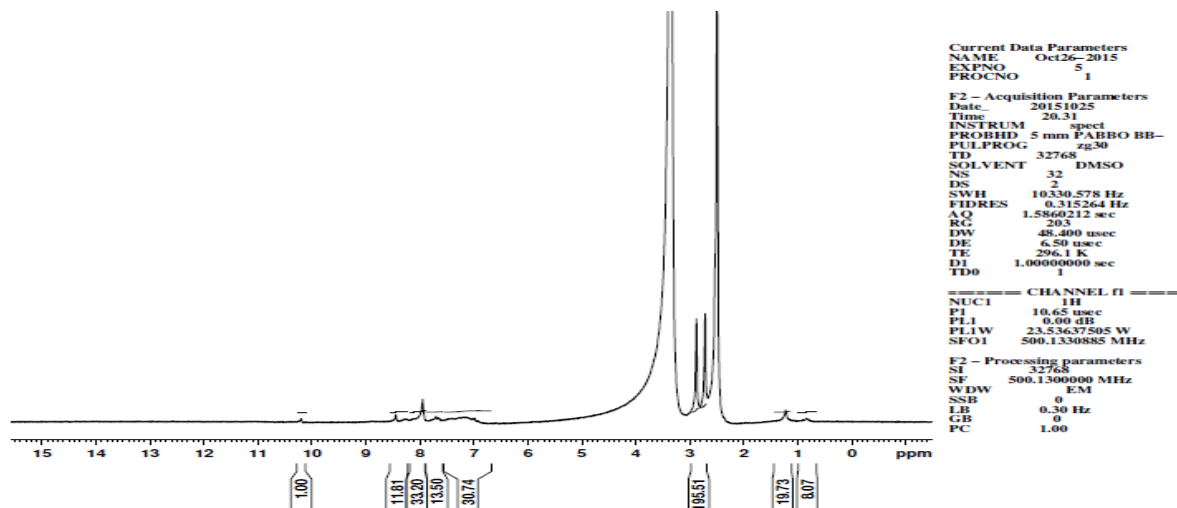


Fig. 9. ¹H Spectrum of the ligand.

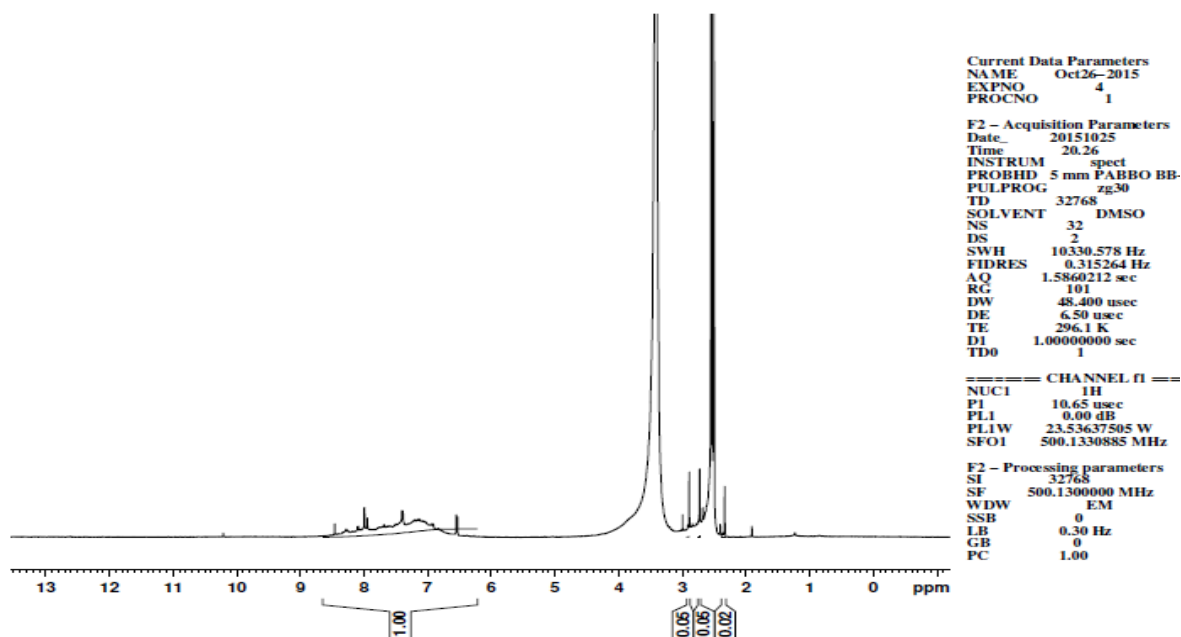


Fig. 10. ¹H Spectrum of the Zn(II) complex

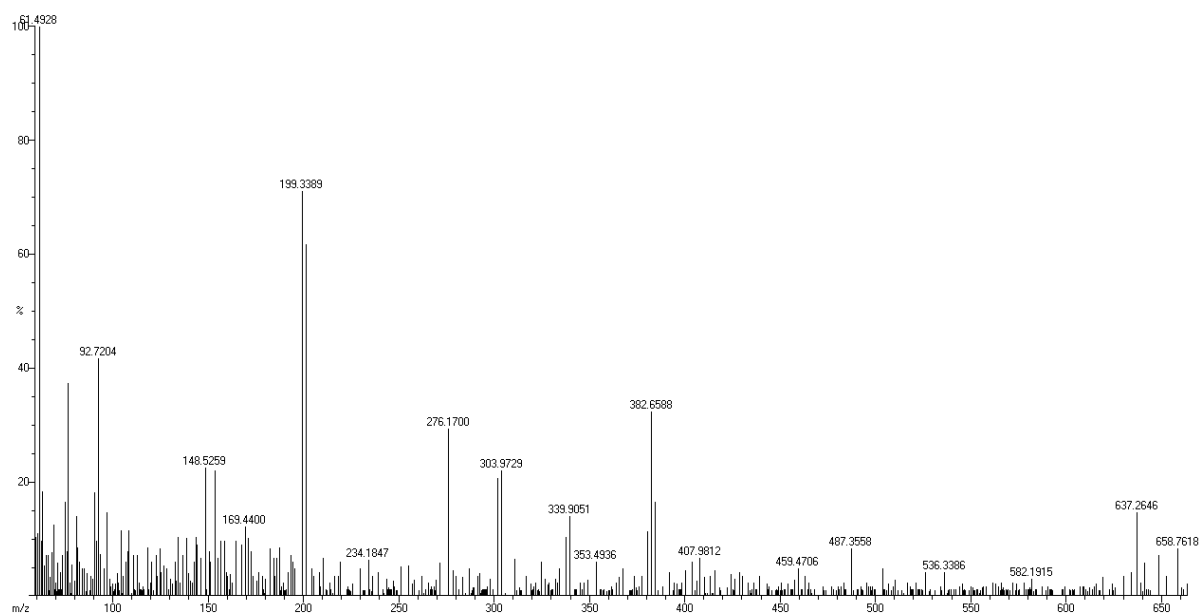


Fig. 11. Mass Spectrum of the ligand

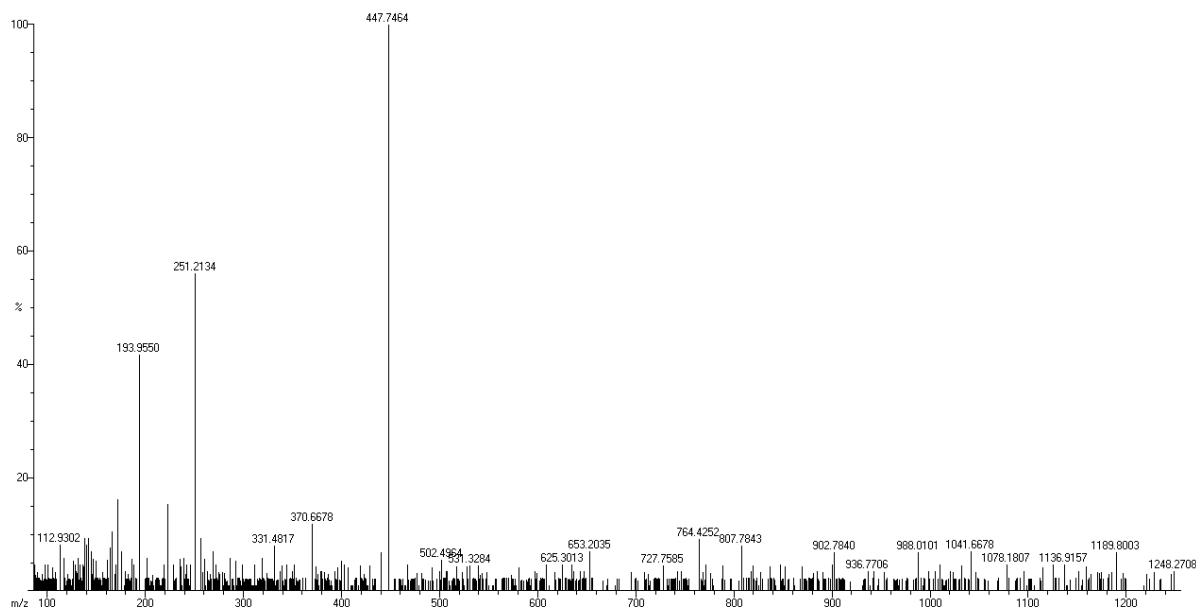


Fig. 12. Mass Spectrum of the Co(II) complex.

ESR spectra

The ESR spectrum of the Cu(II) (Fig. 13) complex was recorded at room temperature to study nature of bonding between the Cu(II) ion and donor atoms of the ligand. The spectrum shows that g_{\parallel} value is 2.16 and g_{\perp} is 2.05. As the $g_{\parallel} > g_{\perp} > 2.0023$, the unpaired electron is localised in $d_{x^2-y^2}$ orbital of the Cu(II) ion and axial symmetry tetragonal geometry of the complex is implied[27]. This is confirmed by the electronic spectrum of the complex. The observed value of G was found to be 3.2 by using the relation $G = g_{\parallel} - 2 / g_{\perp} - 2$ which suggests exchange interaction between the copper centres in a polycrystalline solids[28]. The g_{av} value of the complex is calculated as 2.086 by using the relation $g_{av} = 1/3(g_{\parallel} + 2g_{\perp})$. The spin-orbit coupling constant is also calculated by using the equation $g_{av} = 2(1 - 2\lambda/10dq)$ and it is found to be -660.05 cm^{-1} . This value is found to be less than the free ion value (-830 cm^{-1}) that indicates overlapping of metal-ligand orbitals[29]. The covalent bonding between metal ion and orbitals of the ligand is also confirmed from the g_{\parallel} value, According to Kivelson and Neiman covalent bonding can be predicted for a Cu(II) complex with g_{\parallel} value less than 2.3[30]. Hence, distorted octahedral geometry may be proposed for the Cu(II) complex.

Thermogravimetric study

The thermo gravimetric study of the Ni(II) (Fig. 14, 15) complex as a representative member of the investigating complexes was carried out by the simultaneous TG,DTG and DSC techniques in the atmosphere of nitrogen at a rate of $10 \text{ }^{\circ}\text{C}$ per minute from the ambient temperature to $1400 \text{ }^{\circ}\text{C}$. The TG /DTG curves show that the complex suffers mass loss in a number of stages. The complex loses a mass of 13.39 % at $82.2 \text{ }^{\circ}\text{C}$ in the first stage, with an endothermic peak at $85 \text{ }^{\circ}\text{C}$ in the DSC curve which corresponds to the loss of lattice held water. In the second stage, it suffers a mass of 12.60 % at $341.6 \text{ }^{\circ}\text{C}$ corresponding to the loss of coordinated water with a endothermic peak at $312 \text{ }^{\circ}\text{C}$. The complex compound loses a mass of 27.09 in the third stage which corresponds to the loss of ligand moiety and chlorine atoms at $565 \text{ }^{\circ}\text{C}$ with an endothermic peak $580 \text{ }^{\circ}\text{C}$. The complex suffers a total mass of 62.78 % and its remaining residual mass consisting of NiO as the residue is 37.22% up to $1400 \text{ }^{\circ}\text{C}$. This study indicates thermal stability of the complex.

XRD study

The XRD(powder pattern) study of the Cu(II) complex given in Fig. 16, Table 4 and Ni(II) complex given in Fig. 17, Table 5 was made to determine their crystal system. The X-ray powder diffraction diagram was collected from the X'Pert diffractometer and the recording conditions are 40 kv and 40 mA for $\text{CuK}\alpha$ with $\lambda = 1.542 \text{ \AA}$ between 20° to 80° with a step size of 0.0089° .

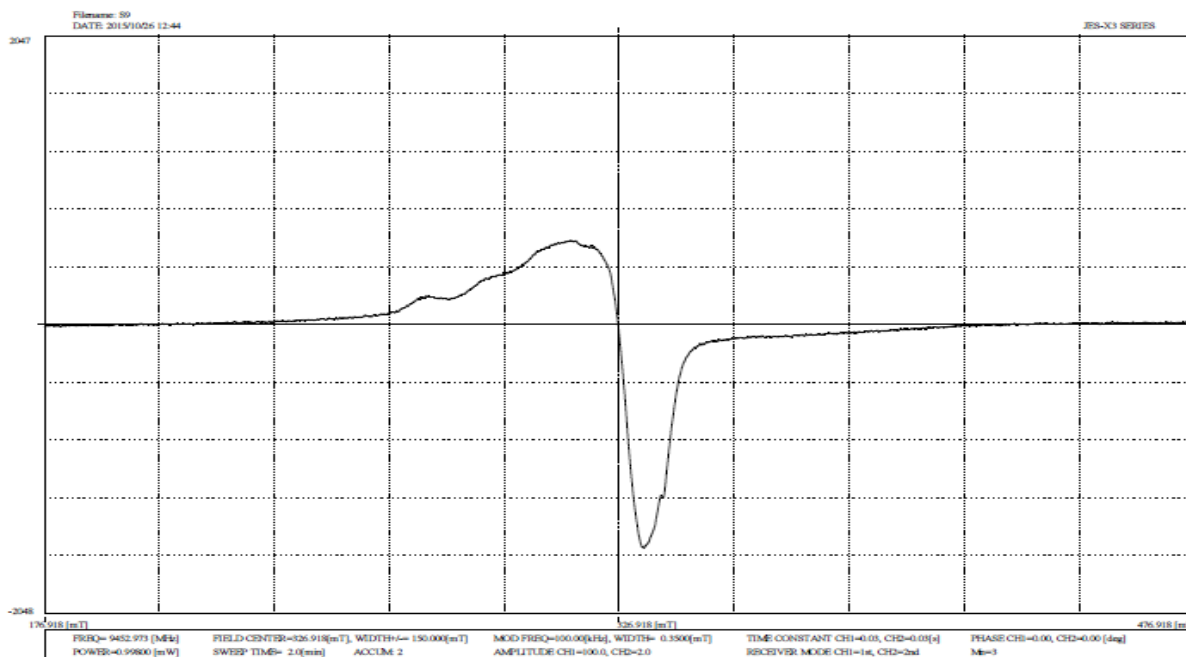


Fig. 13. ESR Spectrum of the Cu(II) complex.

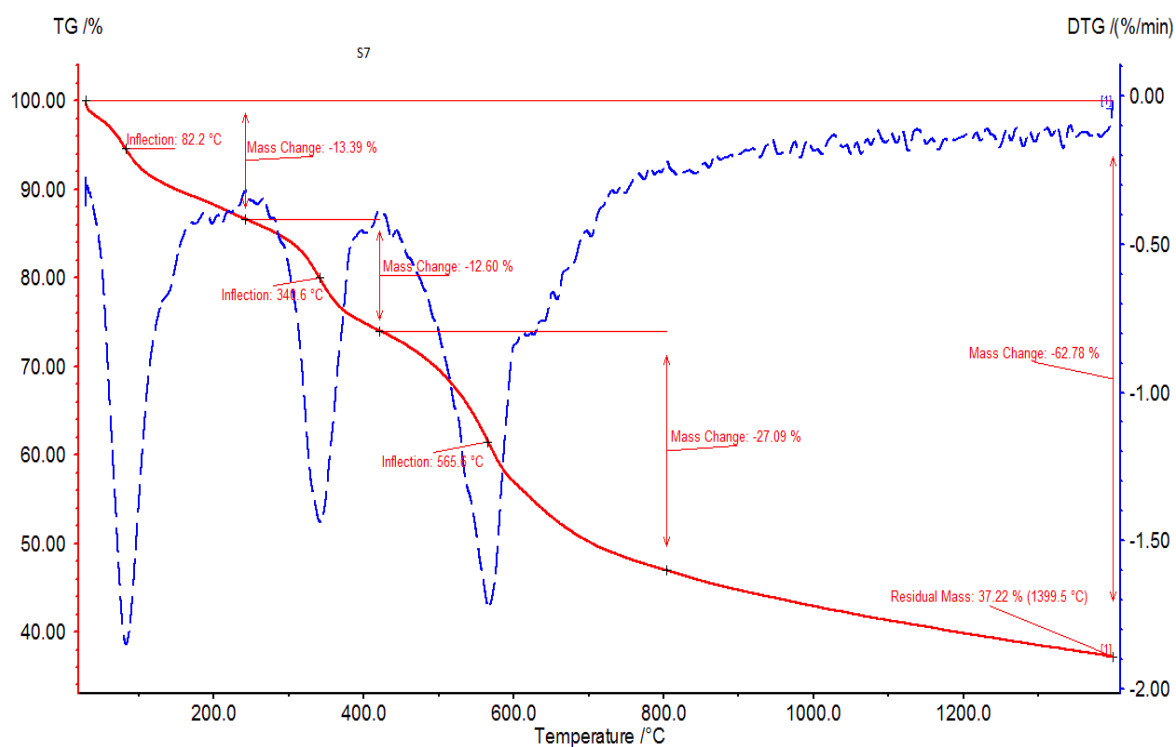


Fig. 14. TG/DTG Graph of Ni(II) complex.

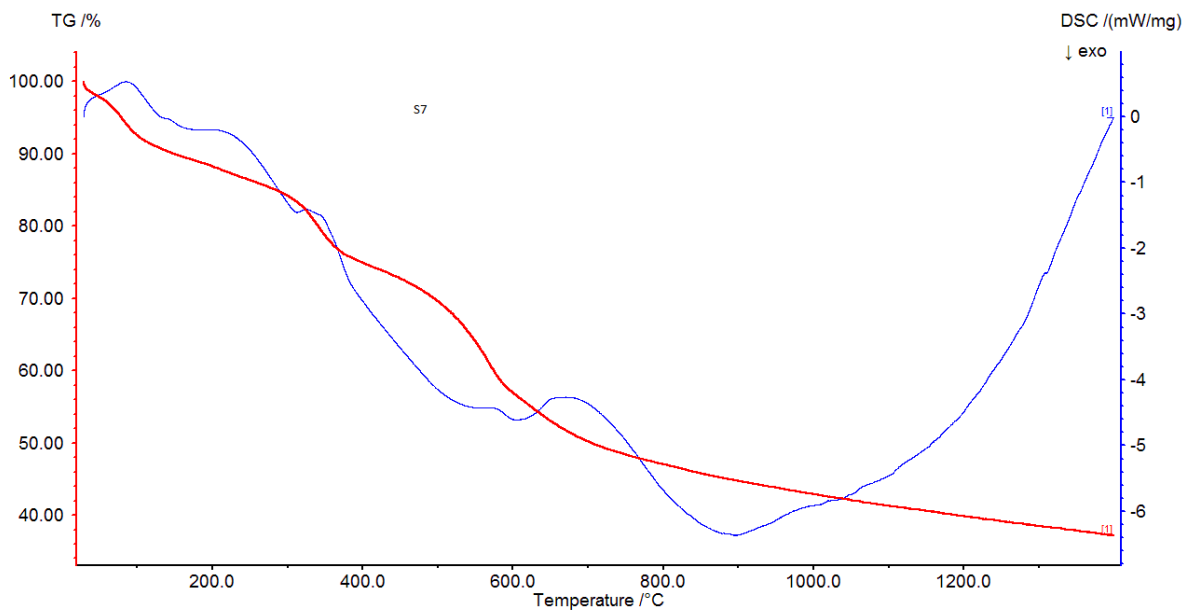


Fig. 15. DSC Graph of Ni(II) complex.

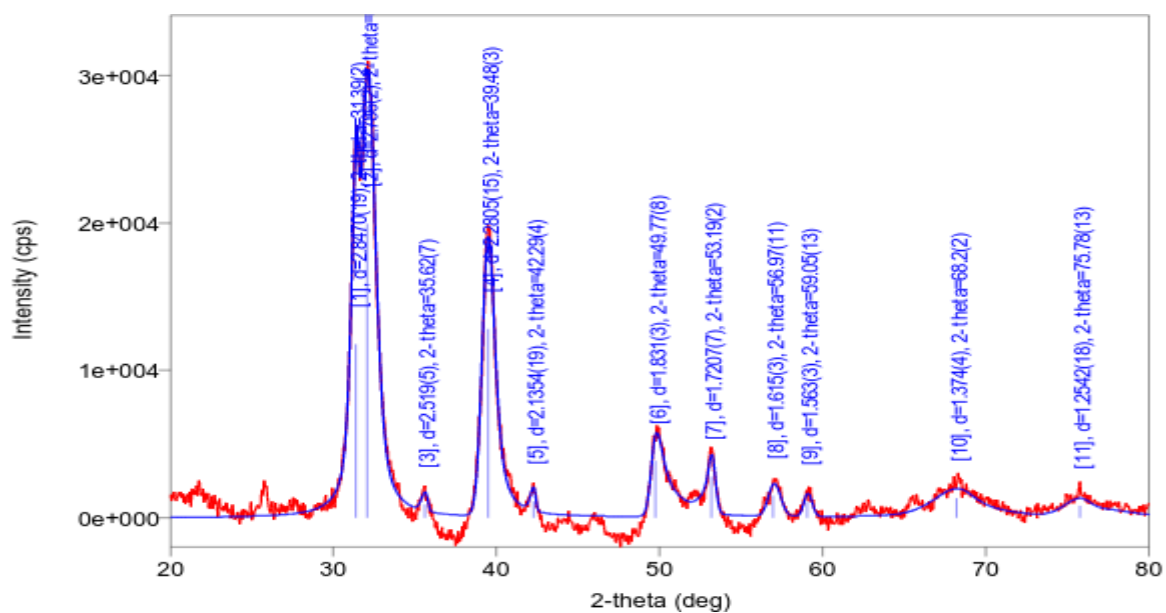


Fig. 16. XRD Powder pattern of the Cu(II) complex.

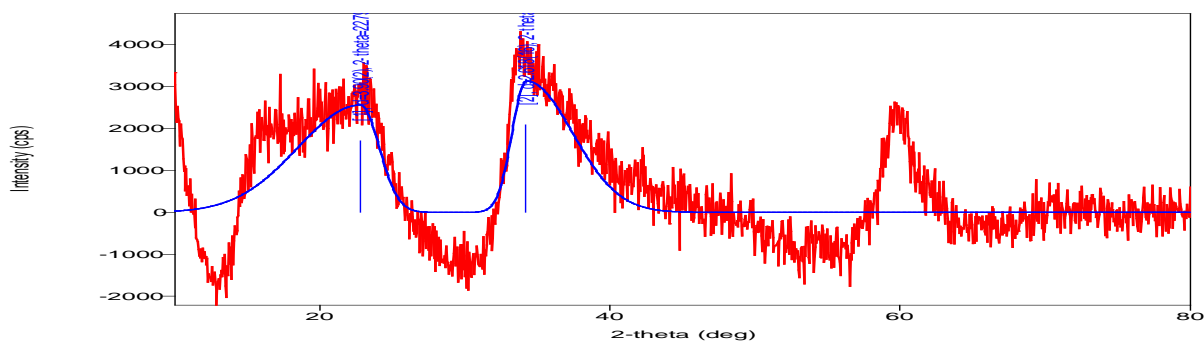


Fig. 17. XRD Powder pattern of the Ni(II) complex.

Table 4. XRD data of the Cu(II) complex at room temperature.

Sl no	2 θ (degree)	d	FWHM(degree)	Intensity(cps degree)
1	31.39(2)	2.8470(19)	0.56(4)	8980(1850)
2	32.10(2)	2.786(2)	1.06(8)	28678(1957)
3	35.62(7)	2.519(5)	0.4(2)	418(254)
4	39.48(3)	2.2805(15)	0.94(3)	15078(384)
5	42.29(4)	2.1354(19)	0.37(12)	463(177)
6	49.77(8)	1.831(3)	1.01(12)	5850(399)
7	53.19(2)	1.7207(7)	0.57(9)	2385(214)
8	56.97(11)	1.615(3)	0.86(10)	1386(178)
9	59.05(13)	1.563(3)	0.57(11)	699(108)
10	68.2(2)	1.374(4)	3.3(3)	6740(334)
11	75.78(13)	1.2542(18)	2.31(18)	3094(231)

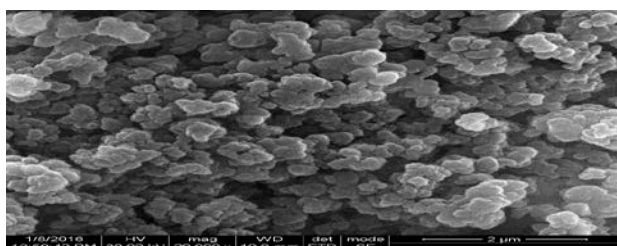
Table 5. XRD data of the Ni(II) complex at room temperature.

Sl no	2 θ (degree)	d	FWHM(degree)	Intensity(cps degree)
1	22.79(15)	3.90(2)	6.6(4)	11979(788)
2	34.2(2)	2.618(16)	4.49(2)	10912(742)

The XRD powder pattern was processed in X'pert high score software package. The search matching procedure was adopted for the PXRD pattern for the Cu(II) complex and revealed a match with a copper compound corresponding JCPDS powder diffraction file with PDF No 751765 . The pattern can be indexed to be a orthorhombic crystal system with $a=14.25$, $b=22.68$, $c=13.50$, $\alpha=\beta=\gamma=90^\circ$, lattice-primitive and space group is Ccca. Similarly, the search matching procedure is repeated for Ni(II) complex that provided a match with a Nickel compound corresponding JCPDS powder diffraction file with PDF No 451027 and the pattern is indexed to be a Hexagonal crystal system with lattice primitive and space group $P6_3/mmc$.

Surface morphology study

The surface morphology study of the Zn(II) complex of the ligand as a representative of all complexes was undertaken to evaluate its morphology and particle size. It is seen from the SEM image of the complex as given in Fig. 18 that the size of the particles is 2 μm with the formation single phase morphology. It is also noticed that there is a uniform matrix of the synthesized complex and the complex shows a flower like shape consisting of particles with nanosized grain.

**Fig. 18.** SEM image of Zn(II) complex

Fluorescence study

The fluorescence study of the ligand (Fig. 19) and its Cu(II) complex (Fig. 20) were carried out to study the photoconductive nature of the investigated compounds and the emission spectra of the compounds were given here. The ligand shows a emission maximum wavelength at 400 nm but the Cu(II) complex depicts the emission maximum wavelength at 420 nm. The red shift of the λ_{max} value of the complexes may be due to the deprotonation of the (-OH) group. The fluorescence intensity of the complex is more than the ligand due to complexation as it enhances conformational rigidity and non-radiative energy loss[31]. The emission in the complexes may be due to intraligand $\pi - \pi^*$ transition. These findings suggest that both the ligand and its complex are fluorescent in nature[32].

Computational study

A computational study of the investigating compounds was made to examine their reactivities and to evaluate geometrical parameters. Gauss view 4.1[33] and chemcraft software are used to draw the structures. The structures of the ligand and its all metal complexes are optimised at B3LYP[34] level of theory using 6-311++G(d,p) basis set. 6-311++G(d,p) is a large basis set which include diffused and polarised wave functions to take in to account the characteristics associated with ionic species having heavy atoms like N. The harmonic frequency calculation is also carried out at the same level of theory to ensure that the structures are true minima. Optimised was performed without any symmetry constraint using the default convergence criteria provided in the software.

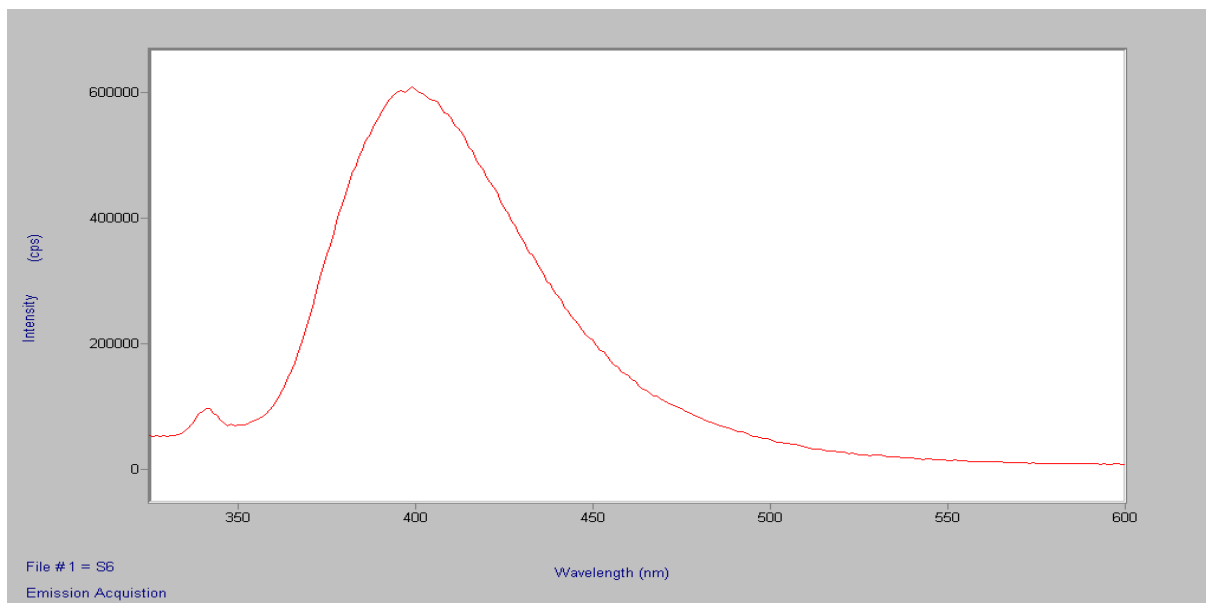


Fig. 19. Emission Graph of ligand.

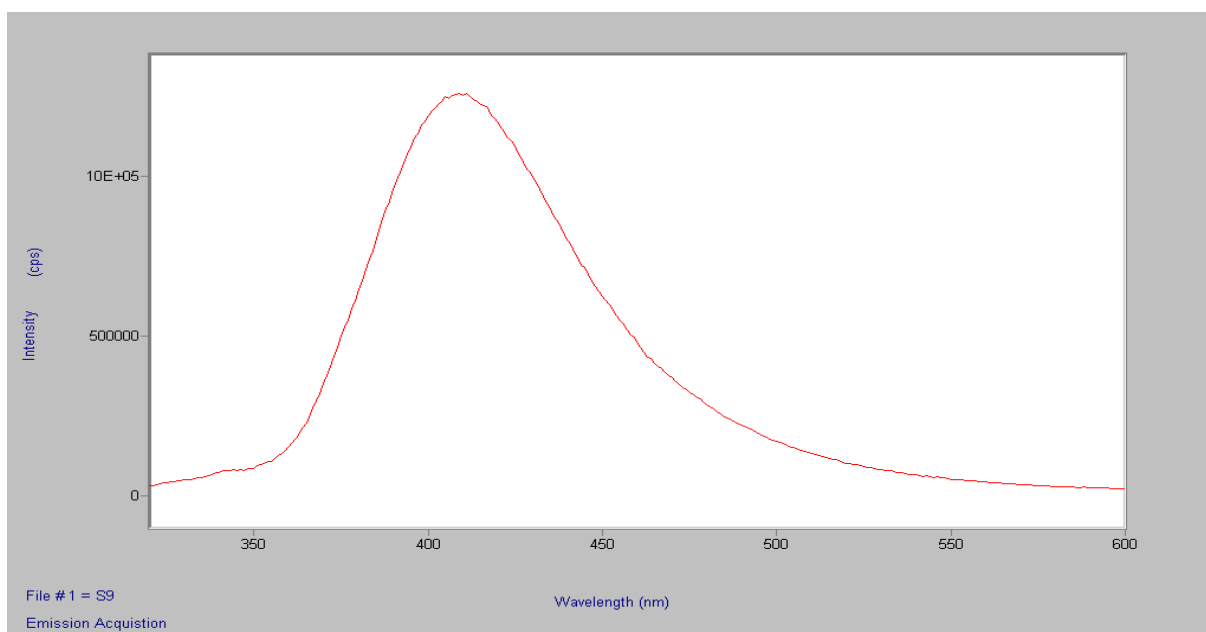


Fig. 20. Emission Graph of Cu(II) complex.

Conceptual DFT defines chemical potential μ as the first derivative of energy with respect to number of electrons

$\mu = \left(\frac{\partial E}{\partial N}\right) \vartheta(r)$ where E = energy, N = number of electrons of the system at constant external pressure $\vartheta(r)$.

and chemical hardness n as the half of the second derivative of energy with respect to number of electrons, so chemical hardness will be the first derivative of energy with respect to number of electrons

$$n = \frac{1}{2} \left(\frac{\partial \mu}{\partial N}\right) \vartheta(r)$$

But chemical potential(μ) and chemical hardness(n) were also calculated in most cases in

terms ionisation potential(IP) and electron affinity(EA) and therefore

$$\mu = -\left(\frac{IP+EA}{2}\right) \text{ and } n = \left(\frac{IP-EA}{2}\right)$$

According Koopman's theorem, IP and EA are related to energies of the Highest occupied molecular orbital(E_{HOMO}) and Lowest occupied molecular orbital(E_{LUMO}) in this way

$$IP = -E_{HOMO} \text{ and } EA = -E_{LUMO}$$

$$n = \left(\frac{E_{LUMO}-E_{HOMO}}{2}\right) \text{ and } \mu = \left(\frac{E_{LUMO}+E_{HOMO}}{2}\right)$$

and Parr and co-workers proposed electrophilicity[35] as a measure of electrophilic

power of a compound the electrophilicity can be represented as

$$\omega = \frac{\mu^2}{2n}$$

The chemical potential(μ) and chemical hardness(n), electrophilicity and dipole moment of the ligand and complexes are given in the table-6. The reactivity of the ligand and its metal complexes can be predicted by considering the minimum electrophilicity principle. According to minimum electrophilicity principle, compound having minimum electrophilicity will have maximum stability. The chemical potential(μ), chemical hardness(n), electrophilicity(ω) were calculated from the HOMO and LUMO value of the ligand and its complexes (Fig. 21) and presented in the table 6.

The geometrical parameters of the investigating compounds were also collected from their optimised geometry (Fig. 22, 23) and presented in the table 7. It is seen from the table that the bond angles around the metal ion in case of Co(II), Ni(II) and Cu(II) complexes are close to 90° and in case of Zn(II), it is close to 109°. Therefore, distorted octahedral geometry for Co(II), Ni(II) and Cu(II) complexes and distorted tetrahedral geometry may be suggested for the Zn(II) complex.

Non-linear optical properties

The electronic properties of chemical compounds are related to their non-linear optical activities. Easy electron transition between molecular orbitals is the basic requirement for good nonlinear optical materials. It is seen from the Table-6 that all metal complexes except Zn(II) complex have higher dipole moment than the free ligand. The energy gap between the HOMO and LUMO of the ligand is found to be higher than the complexes. All these findings indicate that complexes have better nonlinear optical properties[36] than the free organic ligand. The Cu(II) complex will be the good nonlinear optical material due to small energy gap between its HOMO and LUMO and high dipole moment.

BIOLOGICAL EVALUATIONS

Antibacterial studies

All the test compounds were screened against the gram-positive and gram negative bacterial (Table 8, Fig. 24). The ligand and some complexes have moderate effect on the growth of the microorganism. The complexes have more antibacterial abilities than the free ligand and the enhanced ability of the complexes may be explained by considering overtone's concept and chelation theory [37].

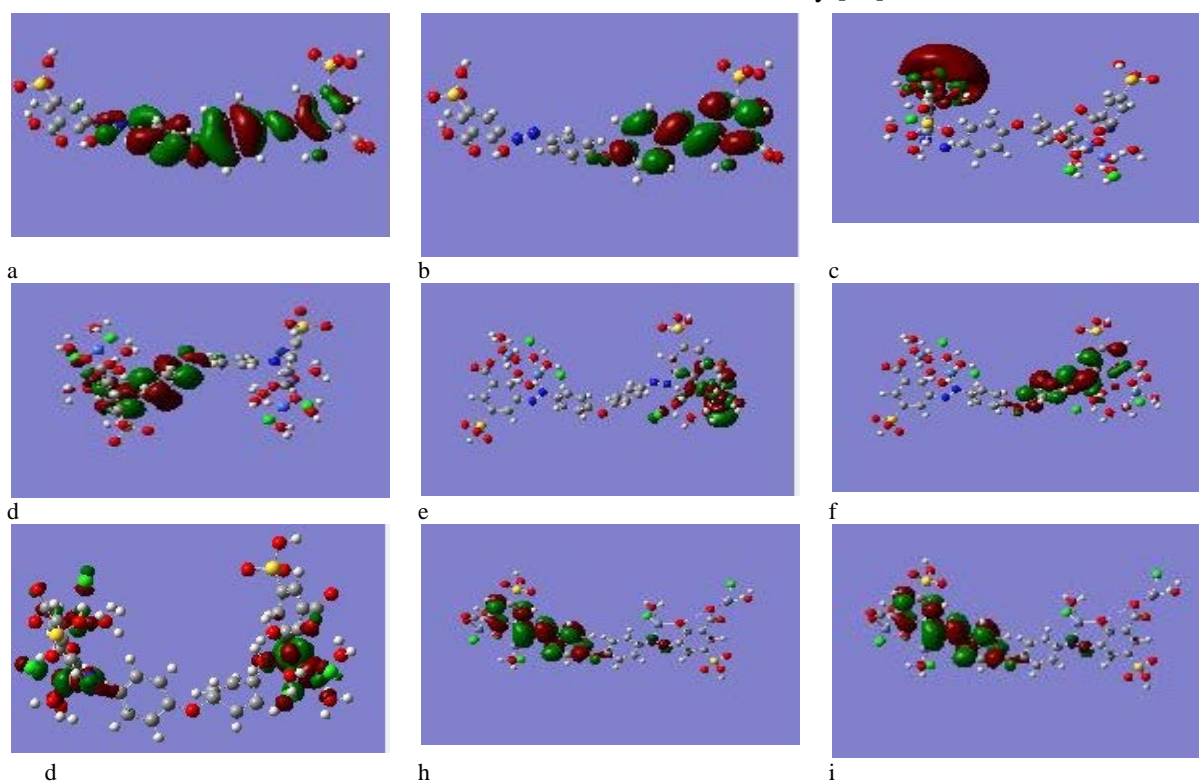


Fig. 21. HOMO and LUMO of the ligand a) HOMO of the ligand; b) LUMO of the ligand; c) LUMO of the Co(II) complex; d) HOMO of the Co(II) complex; e) HOMO of the Ni(II) complex; f) LUMO of the Ni(II) complex; g) HOMO of the Cu(II) complex; h) HOMO of the Zn(II) complex; i) LUMO of the Zn(II) complex.



Fig. 22. Optimised geometry of the Ni(II) complex

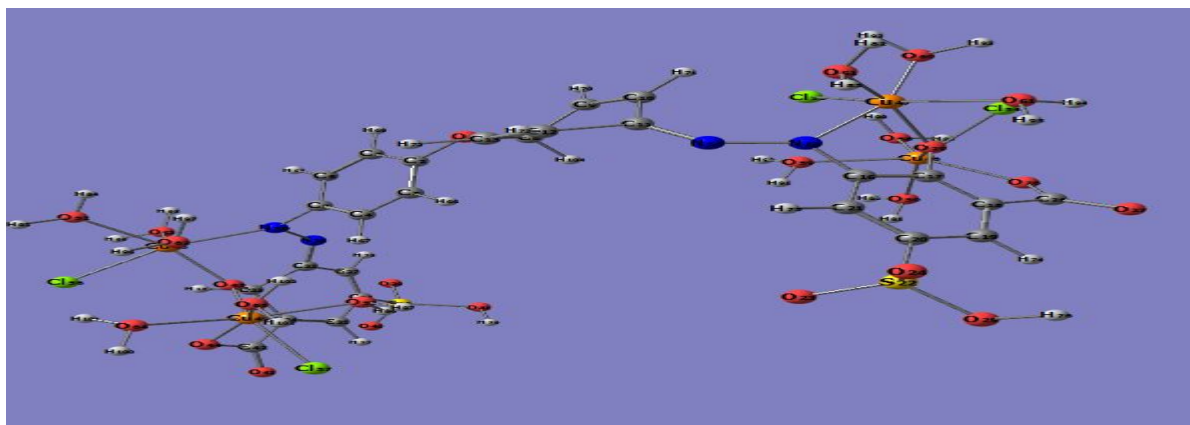


Fig. 23. Optimised geometry of the Cu(II) complex

Table 6. Reactive descriptors of the ligand and its complexes.

Compound	E _{HOMO} (eV)	E _{LUMO} (eV)	μ(eV)	n(eV)	η(eV)	Dipole moment(B.M.)
LH ₄	-0.33549	0.01561	-0.1599	0.1755	0.072	8.194
[Co ₄ LCl ₄ (H ₂ O) ₁₂]	-0.17651	0.00380	-0.086	0.090	0.041	14.592
[Ni ₄ LCl ₄ (H ₂ O) ₁₂]	-0.30137	-0.01775	-0.1595	0.1418	0.089	25.544
[Cu ₄ LCl ₄ (H ₂ O) ₁₂]	-0.11799	-0.07763	-0.097	0.0201	0.234	29.54
[Zn ₄ LCl ₄ (H ₂ O) ₄]	-0.34638	-0.02249	-0.1844	0.1619	0.1050	4.9775

Table 7. Selected bond length and bond angle

comp	Bondlength(A ⁰)				Bondangle(°)	
	N(14)-N(15)	N(15)-C(16)	O(28)-C(27)	N(15)-M(47)-O(29)	N(15)-M(47)-O(60)	N(15)-M(47)-Cl(55)
1	1.232	1.445	1.352	-	-	-
2	1.273	1.483	1.351	87.779	96.927	84.565
3	1.273	1.481	1.350	87.769	96.926	84.561
4	1.274	1.416	1.373	75.431	91.848	96.578
5	1.244	1.462	1.347	86.938	107.854	101.008

1.LH₂, 2.[Ni₄LCl₄(H₂O)₁₂], 3.[Cu₄LCl₄(H₂O)₁₂], 4. [Zn₄LCl₄(H₂O)₄]

Table 8. Antibacterial Screening of the investigating compounds.

compound	Concentration	<i>E. coli</i>	<i>S. aureus</i>
1.LH ₄	500 μg/ml	9	12
2.[Co ₄ LCl ₄ (H ₂ O) ₁₂]	500 μg/ml	14	13
3.[Ni ₄ LCl ₄ (H ₂ O) ₁₂]	500 μg/ml	10	14
4.[Cu ₄ LCl ₄ (H ₂ O) ₁₂]	500 μg/ml	12	12
5.[Zn ₄ LCl ₄ (H ₂ O) ₄]	500 μg/ml	10	11
6.Tetracycline	500 μg/ml	30	30

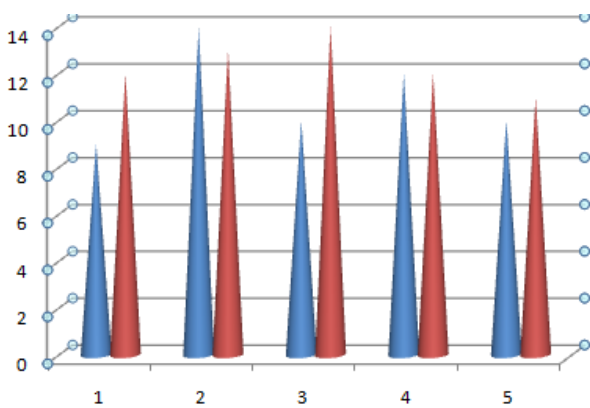


Fig. 24. Antibacterial Screening of the investigating compounds

Gel electrophoresis

The interaction between complex and metal complexes was also studied by gel electrophoresis as given in Fig. 25. The electrophoresis study shows that intensity of the DNA-complex bands are less than the DNA control and the intensity decreases in the order of $[\text{Cu}_4\text{LCl}_4(\text{H}_2\text{O})_{12}] > [\text{Ni}_4\text{LCl}_4(\text{H}_2\text{O})_{12}] > [\text{Co}_4\text{LCl}_4(\text{H}_2\text{O})_{12}]$ (lane 2- Co(II) complex, lane 3 – Ni(II) complex, lane 4- Cu(II) complex and lane 1- DNA CONTROL . Due to the intercalation of the metal complexes in to the DNA base pairs, intensity decreases

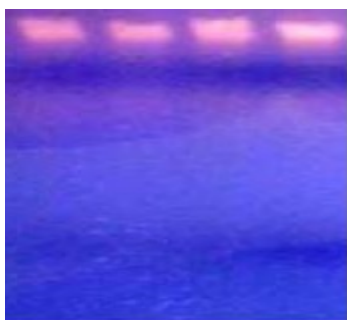


Fig. 25. Intensity of the DNA-complex: from left - 1. $[\text{Cu}_4\text{LCl}_4(\text{H}_2\text{O})_{12}]$, 2. $[\text{Ni}_4\text{LCl}_4(\text{H}_2\text{O})_{12}]$, 3. $[\text{Co}_4\text{LCl}_4(\text{H}_2\text{O})_{12}]$, 4. DNA control

Viscosity measurement test

All the metal complexes are subjected to viscosity measurement study to confirm the DNA binding abilities of the metal complexes with the CT DNA. The increase in viscosity of DNA occurs when the complexes intercalate between the base pairs due to extension in the helix[38]. The effects of all the synthesised complexes on the viscosity of DNA are shown in Fig.26. The graph shows that viscosity of DNA increases with increase in the concentration of complexes and the order of increase of viscosity is $[\text{Cu}_4\text{LCl}_4(\text{H}_2\text{O})_{12}] > [\text{Ni}_4\text{LCl}_4(\text{H}_2\text{O})_{12}] > [\text{Zn}_4\text{LCl}_4(\text{H}_2\text{O})_4] > [\text{Co}_4\text{LCl}_4(\text{H}_2\text{O})_{12}]$.

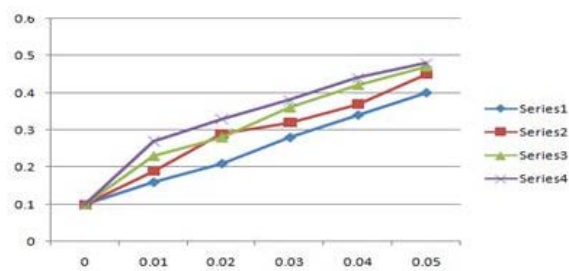


Fig. 26. $(\eta/\eta_0)^{1/3}$ verses $[\text{complex}]/[\text{DNA}]$ Series: 1- $[\text{Cu}_4\text{LCl}_4(\text{H}_2\text{O})_{12}]$, 2- $[\text{Ni}_4\text{LCl}_4(\text{H}_2\text{O})_{12}]$, 3- $[\text{Zn}_4\text{LCl}_4(\text{H}_2\text{O})_4]$, 4- $[\text{Co}_4\text{LCl}_4(\text{H}_2\text{O})_{12}]$.

CONCLUSION

On the basis various physico-chemical and spectral data presented and discussed, the ligand acted as a hexa dentate ligand as it coordinated with the metal atoms through OON-NOO donor atoms. Distorted octahedral geometry for the Co(II), Ni(II), Cu(II) and distorted tetrahedral geometry for Zn(II) is proposed on the basis of analytical, spectral data and computational study. Thermal study of the metal complex indicates thermal stability of the complexes, the fluorescence studies reveals that both ligand and its metal complexes have fluorescent properties and can be used for making photo conducting materials. The ligand and its complexes are known to have antibacterial properties and DNA binding abilities as indicated from their biological studies.

Acknowledgements: Author acknowledges UGC for financial support in the form of Minor Research Project(F.PSO-4/13-14(ERO) and SAIF, IIT ,CHENNAI for providing spectral data.

REFERENCES

1. A.T. Peters, H.S. Freeman, Colour chemistry, the design and synthesis of organic dye and pigments, Elsevier App. Sci. Publications, 1991.
2. A.M. Khedr, M. Gaber, R.M. Issa, H. Erten, *Dyes Pigm.*, **67**, 117 (2005).
3. F. Arjmand, M. Muddasir, *J. of Photochem. Photobiol. B Biol.*, **101**,37 (2010).
4. F. Arjmand, B. Mohani, S. Ahmed, *Eur. J. Med. Chem.*, **40**, 1103 (2005)
5. K. Nejati, Z. Rezvani, B. Massoumi, *Dyes Pigm.*, **75**, 653 (2007)
6. M. Tumer, D. Ekinci, F. Tumer, A. Bulut, *Spectrochim. Acta Part A Mol. Biomol. Spectroscopy*, **67**, 916 (2007).
7. S. Rai, A. Bajpai, S. Lokhandwala, *Adv. Mat. Lett*, **5**(4), 206 (2014).
8. C. Selvi, D. Nartop, *Spectrochim Acta A Mol. Biomol. Spectroscopy*, **95**, 165 (2012).

9. F. Frisch, G. Trucks, H. Schlegel, G. Scuseria, M. Robb, J. Cheeseman, J. Montgomery, T. Ureven, K. Kudin, J. Burant, Gaussian 03 Rev B. 03, Gaussian Inc, Pittsburg, PA, 2003.
10. D. Sobolova, M. Kozurkova, T. Plichta, Ondrusova, Z. Simkovic, M.H. Paulikova, A. Valent, *International Journal of Biological Macromolecules*, **48**, 319 (2011).
11. L. H. Abdel-Rahman, R. M. El-Khatib, L.A. E. Nassr, A.M. Abu-Dief, F. El-Din Lashin, *Spectrochimica Acta Part A: Molecular Biomolecular Spectroscopy*, **111**, 266 (2013).
12. R.S. Brant, E.R. Miller, *J. Bacteriol.*, **38**(5), 525 (1939).
13. W.J. Geary, *Coord. Chem. Rev.*, **7**, 81 (1971).
14. A. Saxena, J.P. Tondon, *Polyhedron*, **3**, 681 (1984).
15. S.D. Robinson, M.F. Uttley, *J. Chem. Soc.*, **2**, 1912 (1973).
16. R.B. King, *Inorganic Chemistry*, **5**, 300 (1961).
17. V. Stefov, V. M. Petrusevski, V. M. Soptrajanov, *B. J. Mol. Structure*, **97**, 2939 (1961).
18. K. Nakamoto, *Infrared and Raman Spectra of Inorganic and Coordination compounds*, Wiley and sons, 2009.
19. A.B.P. Lever, *Coord. Chem. Rev.*, **3**, 119 (1968).
20. M. Shakir, A.K. Mahammed, O.S.M. Nasman, *Polyhedron*, **15**, 3487 (1996).
21. P.P. Dholakiya, M.N. Patel, *React. Inorg. Met. Org. Nano-Met. Chem.*, **32**, 819 (2002).
22. S. Yamada, *Coord. Chem. Rev.*, **1**, 445 (1966).
23. A.B.P. Lever, E.I. Solomon, *Inorganic Electronic Structure and Spectroscopy*, Wiley and sons, 2014.
24. M.K.S. Abou, H. Faruk, *J. of Iran Chem. Soc.*, **5**, 122 (2008).
25. D.H. Williams, I. Fleming, *Spectroscopic methods in organic chemistry*, Tata McGraw Hill, 1994.
26. A.E. Ahmed, Taha, M.A. E. *Spectrochimica Acta Part A: Molecular Biomolecular Spectroscopy*, **56**, 2775 (2011).
27. A.F.M. Benial, V. Ramakrishan, R. Murugesan, *Spectrochimica Acta Part A: Molecular Biomolecular Spectroscopy*, **79**, 1803 (2000).
28. B.J. Hathaway, D.E. Billing, *Coord. Chem. Rev.*, **5**, 143 (1970).
29. R.L. Dutta, A. Syamal, *Elements of Magnetochemistry*, East-West Press PVT LTD, 2010.
30. D. Kivelson, R.R. Neiman, *J. Chem. Phys.*, **35**, 159 (1970).
31. C. Anita, C.D. Sheela, P. Tharmaraj, S. Sumati, *Spectrochimica Acta Part A: Molecular Biomolecular Spectroscopy*, **96**, 493 (2012).
32. A. Majumdar, G.M. Rosair, A. Mallick, N. Chattopadhyaya, S. Mitra, *Polyhedron*, **25**(8), 1753 (2006).
33. R. Dennington, T. Keith, J. Milliam, *Gauss View Version 4.1*, 2007.
34. A.D. Beckel, *J. Chem. Phys.*, **98**, 564 (1993).
35. R.J. Parr, R.J. Pearson, *J. Am. Chem. Soc.*, **75****12**, 105 (1983).
36. S.M. Soliman, M. A.M. Abu-Youssef, J. Albering, A. El-Faham, *J. Chem. Sci.*, **12**, 2137 (2015).
37. A.B.P. Lever, *Journal of Molecular Structure*, **129**, 180 (1985).
38. P.R. Hertzberg, P.B. Dervan, *J. Am. Chem. Soc.*, **104**, 313 (1982).

СИНТЕЗА, СПЕКТРОСКОПСКО ОХАРАКТЕРИЗИРАНЕ И БИОЛОГИЧНА АКТИВНОСТ НА Co(II), Ni(II), Cu(II) И Zn(II) МЕТАЛНИ КОМПЛЕКСИ С ЛИГАНДИ ОТ АЗО-БАГРИЛО, ПОЛУЧЕНО ОТ 4,4'-ДИАМИНОДИФЕНИЛЕТЕР И 5-СУЛФОСАЛИЦИЛОВА КИСЕЛИНА

С.Н. Чаулия

Департамент по химия, Г.М. Колеж, Самбалтур, Одиша, Индия

Постъпила на 16 февруари, 2016 г.; коригирана на 27 май, 2016 г.

(Резюме)

Синтезирани са серия от метални комплекси на Co(II), Ni(II), Cu(II) и Zn(II) с нови лиганди от азо-багрило 4,4'-bis(2'-хидрокси-3'-карбокси-5'-сулфофенил-азо)дифенил етер, получено от 4,4'-диаминофенил етер и 5-сулфосалицилова киселина. Металните комплекси и лигандите са охарактеризирани чрез аналитични методи (ИЧ- и ЯМР-спектроскопия, мас-спектрометрия, електронни спектри) и измервания на моларната проводимост, магнитна чувствителност и термични измервания. Аналитичните и спектралните данни предсказват октаедрична геометрия за комплексите на Co(II) и Ni(II), деформирана октаедрична геометрия за комплекса на Cu(II) и тетраедрична геометрия на комплекса на Zn(II). Проведени са числени изследвания на лигандите и металните комплекси за определянето на геометричните параметри и на общите реактивни дескриптори. Рентгено-структурният анализ на прахови образци показва орто-ромбична кристална система за комплекса на Cu(II). Термичните изследвания разкриват термична стабилност на комплексите, а флуоресцентните изследвания предвиждат фотоактивни свойства на азо-съединенията. Снимките на Zn(II)-комплексите от сканираща електронна микроскопия дават информация за тяхната повърхностна морфология. Биологичното изследване разкрива анти-бактериални свойства и ДНК-свързваща активност на синтезираните съединения.